Progressive differentiation of memory CD8 T cells in the cervicovaginal tissue

Veronica Davé[1,2], E. Fabian Cardozo-Ojeda[1], Florian Mair[1], Jami Erickson[1], Amanda S. Woodward-Davis[1], Andrew Soerens[1], Julie Czartoski[1], Candice Teague[1], Susanne Oberle[3], Dietmar Zehn[3,†], Joshua T. Schiffer[1,4,5], Jennifer Lund[1,2,*], Martin Prlic[1,2,6*]

[1] Vaccine and Infectious Disease Division, Fred Hutchinson Cancer Research Center, Seattle, WA 98109

[2] Graduate Program in Pathobiology, Department of Global Health, University of Washington, Seattle, WA 98195

[3] Division of Immunology and Allergy, Department of Medicine, Lausanne University Hospital, 1011 Lausanne, Switzerland

[4] Clinical Research Division, Fred Hutchinson Cancer Research Center, Seattle, WA 98109

[5] Department of Medicine, University of Washington, Seattle, WA 98195

[6] Department of Immunology, University of Washington, Seattle, WA 98195

Running title: Cervicovaginal CD8 T cell memory

[*]Co-corresponding authors (jlund@fredhutch.org, mprlic@fredhutch.org)

[†]Present address: Division of Animal Physiology and Immunology, School of Life Sciences Weihenstephan, Technical University of Munich, 85354 Freising, Germany

Abstract

The memory CD8 T cell compartment in human cervicovaginal tissue (CVT) is phenotypically and functionally distinct compared to other non-lymphoid tissues. To determine if these distinctive features are driven by residence in the tissue itself, rather than a consequence of local antigenic insults, we used a mouse model to assess memory CD8 T cell differentiation in the CVT. Following systemic immunization to elicit a CD8 T cell response to a herpes simplex virus (HSV) epitope, HSV-specific memory CD8 T cells were stably maintained in other tissues but gradually declined in the CVT over 5 months post-immunization, correlating with a delay in viral control upon HSV challenge. While memory cells in the periphery and small intestine maintained a fairly stable phenotype after 30 days, memory CD8 T cells in the CVT gradually acquired a CD103^{+}, TCF-1^{-}, granzyme B^{+} phenotype over the 5 month time span. Notably, a sizable and phenotypically similar population of CD8 T cells was also found in human CVT. Our data indicate that the CVT environment itself considerably affects memory CD8 T cell maintenance and differentiation, and call for a reassessment of the prevalent model of memory T cell maintenance which does not currently account for tissue-specific divergence.

42 **Introduction**

43 Pathogens that infect mucosal barrier surfaces represent a significant global health
44 burden, yet immune cell function within reproductive mucosal tissues remains understudied. In
45 addition, the phenotypic and functional characteristics of memory T cells in cervicovaginal tissue
46 (CVT) compared to other mucosal and lymphoid organs is poorly understood, despite the
47 potentially broad importance of this cellular population in the context of sexually-transmitted
48 infections.

49 We recently reported that memory CD8 T cells in the human CVT displayed unique
50 phenotypical and functional features including the presence of a subset of $CD69^{-}$ $CD103^{-}$
51 inflammatory CD8 T cells (1). Importantly, the majority of memory CD8 T cells in the CVT of
52 healthy women typically expressed CD103 and CD69, which are biomarkers associated with
53 tissue-residence (2-4), suggesting that most memory CD8 T cells in the human CVT stably
54 reside there. Tissue-residence itself can affect functional and phenotypical properties of T cells
55 (5-13), which is thought to be a consequence of exposure to metabolites, cytokines, and other
56 factors present in the tissue environment in steady state conditions(14, 15) (16). However, it is
57 unclear if the distinctive features of memory CD8 T cells in the CVT are a consequence of
58 recurring local infections and antigenic insults or driven by residence in the tissue itself. To
59 address this question, we used a mouse model system to assess memory CD8 T cell
60 differentiation and maintenance in the CVT. Specifically, we used a systemic immunization
61 strategy to induce HSV-specific memory CD8 T cells. We then tracked these antigen-specific T
62 cells across tissues over time and examined their protective capacity. Our results suggest that
63 residence of memory CD8 T cells in the CVT itself is sufficient to alter their maintenance and
64 differentiation in the absence of recurrent infections or antigenic exposures.

65

66 **Results**

67 *Systemic immunization with LM-gB elicits stable HSV-specific CD8 T cell memory in secondary*
68 *lymphoid organs and the small intestine, but not the CVT*

69 We generated a recombinant strain of *Listeria monocytogenes* that expresses the SSIEFARL
70 peptide derived from HSV glycoprotein B (LM-gB) to elicit a large population of HSV-specific
71 CD8 T cells in mice without priming HSV-specific CD4 T cell or B cell responses (**Fig 1A**).
72 Importantly, we chose this approach so we could specifically interrogate the ability of gB-specific
73 memory CD8 T cells to mediate protection against HSV infection at later time points in the
74 absence of other HSV-specific memory responses. We found that immunized mice mounted a
75 robust CD8 T cell response, with gB-specific T cells making up an average of 36.4% of CD8 T
76 cells in the blood by 1wk after immunization (**Fig 1B**). The gB-specific T cell compartment
77 underwent contraction beyond 1wk post-immunization, constituting an average of 6.7% of CD8
78 T cells in the blood by 1mo post-immunization (**Fig. 1B**).

79 While the number of gB-specific CD8 T cells remained relatively stable in the spleen,
80 dLN and small intestine beyond 1mo after immunization (**Fig. 1C-D**), this population underwent
81 a threefold loss in number within the CVT, with some mice having very few gB-specific CD8 T
82 cells remaining in the CVT by 5 months post-immunization (**Fig. 1D**). These results suggest that
83 memory CD8 T cell maintenance in the CVT might diverge from that in other non-lymphoid
84 tissues.

85

86 *Memory CD8 T cells in the CVT acquire expression of canonical markers of tissue residency*
87 *over time*

88 Given that gB-specific CD8 T cells in the CVT continued to decline in number after T cell
89 contraction had concluded in other lymphoid tissues, we next examined the expression of
90 canonical markers of tissue residency and effector function. To reliably determine what
91 proportion of the gB-specific CD8 T cells in each organ were located within the tissue, we

92 performed intravascular (i.v.) labeling (17, 18) (**Fig. S1**). We found that an average of 85.6% of
93 the gB-specific CD8 T cells in the CVT were protected from i.v. labeling by 1mo after
94 immunization (**Fig. 2A**). The proportion of CVT gB-specific CD8 T cells that were protected from
95 i.v. labeling remained stable across time points, suggesting that the smaller population of T cells
96 remaining at late time points was still composed of cells that were mostly located within the
97 tissue parenchyma (**Fig. 2A**).

98 We next assessed whether gB-specific CD8 T cells expressed CD69 and CD103, two
99 markers often used to indicate tissue residency. Consistent with previous reports (19, 20), we
100 found that these markers were mostly non-expressed on gB-specific CD8 T cells at the earliest
101 memory time point. However, the average frequency of $CD103^+$ cells within the gB-specific CD8
102 T cell subset increased from 20.6% to 54.4% between 1mo and 5mo after LM-gB immunization
103 (**Fig. 2B-D**). While the i.v.-$label^+$ fraction of gB-specific CD8 T cells in the CVT remained almost
104 completely $CD103^-$ for the entire duration of the experiment, the shift from a predominantly
105 $CD103^-$ population to a predominantly $CD103^+$ population was especially clear within the i.v.-
106 $label^-$ fraction of CVT gB-specific CD8 T cells (**Fig. 2C, D**) and was mainly attributable to a loss
107 of $CD103^-$ cells from the CVT over time (**Fig. 2E**). Conversely, the equivalent i.v. $label^-$ fraction
108 of gB-specific CD8 T cells in another mucosal tissue, the small intestine lamina propria (SI LP),
109 did not undergo a population-level shift towards becoming $CD103^+$ (**Fig. 2C**). Finally, the total
110 $CD69^+$ $CD103^+$ population in the CVT was stably maintained over time (**Fig. 2E**), which could be
111 due to conversion of other subsets to a $CD69^+$ $CD103^+$ phenotype or the ability to self-renew at
112 a rate sufficient for stable maintenance.
113
114 *HSV-specific memory CD8 T cells in the CVT slowly change phenotype during the five months*
115 *following immunization*

116 Given the changes we observed in the populations of memory gB-specific CD8 T cells
117 expressing CD69 and CD103 over time (**Fig. 2**), leading to a relative increase in CD103$^+$ cells
118 (**Fig. 2D**), we next wanted to determine if tissue-resident CD8 T cells in the CVT maintain
119 constitutive granzyme B expression similar to the tissue-resident CD8 T cells in the SI LP, which
120 express granzyme B in the absence of antigen re-exposure (21, 22). Few gB-specific CD8 T
121 cells in the CVT expressed granzyme B at 1mo post-immunization (mean: 3%), but the
122 granzyme B$^+$ population substantially increased in both number and frequency at later time
123 points (mean: 24%, **Fig. 3A, B**). By contrast, an average of 17.5% of SI LP gB-specific CD8 T
124 cells expressed granzyme B by 1mo after immunization, and expression remained stable
125 thereafter (**Fig. 3B**). As expected, granzyme B expression was rarely observed among gB-
126 specific CD8 T cells in the spleen or dLN, regardless of the memory timepoint (**Fig. 3B**). We
127 next examined the phenotypic identity of these granzyme B-expressing cells. We found that by
128 3mo post-immunization, granzyme B$^+$ gB-specific CD8 T cells in the CVT were almost
129 exclusively CD103$^+$, suggesting that these two dynamically-expressed markers were
130 demarcating the same cellular population (**Fig. 3C-E**). By contrast, the granzyme B$^+$ population
131 in the SI LP comprised both CD103$^+$ and CD103$^-$ cells (**Fig. 3D-E**). Together, these data
132 suggest that the differentiation of gB-specific memory CD8 T cell compartment in the CVT is not
133 synchronized with gB-specific memory CD8 T cell populations in the gut mucosa or peripheral
134 lymphoid organs.
135
136 *Gene expression analysis of single HSV-specific CD8 T cells from the blood or CVT reveals*
137 *transcriptional differences between early and late memory time points*
138 To assess differences in the CVT gB-specific CD8 T cell compartment at early and late
139 memory timepoints in a more unbiased manner, we FACS-sorted gB tetramer$^+$ cells from the
140 blood and i.v.-label$^-$ gB tetramer$^+$ cells from the CVT at early and late time points for single-cell
141 RNA sequencing (scRNAseq) using a droplet-based microfluidic platform (**Fig. 4A)**. Circulating

142 gB-specific memory CD8 T cells showed an increase in *Sell* (CD62L) and *Il7r* expression in late
143 memory gB tetramer$^+$ cells compared to the early memory time point, while the early time point
144 had higher expression of *Gzma*, *Gzmb*, and *Klrg1,* in line with the shift from effector to central
145 memory that is known to occur over time (23) (**Fig. 4B**). We also looked for transcriptional
146 differences between gB-specific CD8 T cells within the CVT at early and late memory time
147 points. We identified 10 genes that were differentially expressed (Bonferroni-adjusted *P*-value
148 <0.05) between HSV-specific CD8 T cells isolated from the CVT at early memory and late
149 memory time points (**Fig. 4C**). However, most of these genes (*Rps27rt*, *Rps19*, *Rps28*, *Rps5*,
150 *Ccl4*, *S100a4*, *Fth1*) were also differentially expressed in the same direction between blood-
151 derived HSV-specific CD8 T cells at early memory and late memory time points (**Fig. 4B**),
152 suggesting that memory T cells in both the circulation and non-lymphoid tissues undergo these
153 changes. Further, none of these genes differentially expressed by early and late memory CD8 T
154 cells in the CVT were obvious candidates to explain why this compartment declined numerically
155 and changed phenotypically.
156
157 *gB tetramer$^+$ CD103$^+$ CD8 T cells in the CVT lack expression of TCF-1*
158 Given the steady decline of gB tetramer$^+$ T cells in the CVT over time, we examined
159 expression of TCF-1 protein, a transcription factor associated with self-renewal potential in CD8
160 T cells (24), in CD103$^+$ granzyme B$^+$ cells in the CVT (**Fig. 5A-B**). We observed that i.v.-label$^-$
161 CD103$^+$ gB-specific CD8 T cells in the CVT were exclusively TCF-1$^-$ after LM-gB immunization.
162 By contrast, the CD103$^-$ gB-specific T cells in the CVT and dLN were TCF-1^{mid} (**Fig. 5A-B**).
163 Interestingly, CD103$^+$ and CD103$^-$ gB-specific T cells in the SI LP did not express different
164 levels of TCF-1 (**Fig. S2**), again suggesting that memory T cells induced by the same
165 immunization displayed tissue-specific characteristics and may have different requirements for
166 self-renewal. In our scRNA-seq dataset, we likewise observed that *Tcf7* transcript (which

167 encodes TCF-1) was expressed by a significant proportion of gB tetramer$^+$ cells in the blood
168 (**Fig. 5C**), but rarely detected in gB tetramer$^+$ cells isolated from the CVT, regardless of time
169 point. Similar to this finding, the majority of CD103$^+$ CD8 T cells in human vaginal tissue were
170 TCF-1$^-$ (**Fig. 5D**) and expressed lower levels of TCF-1 than memory (CD45RA$^-$) CD8 T cells in
171 matched blood, though this result was not statistically significant (**Fig. 5E**). We additionally
172 observed that most granzyme B$^+$ CD8 T cells in human vaginal tissue co-expressed CD103
173 (**Fig. 5F-G**), also mirroring the phenotype we observed in mouse CVT. These data demonstrate
174 that CD103$^+$ CD8 T cells residing in both mouse and human cervicovaginal tissues express
175 granzyme B and lack TCF-1.
176
177 *Numerical and phenotypical changes of HSV-specific memory T cells in the CVT lead to*
178 *delayed protection against viral challenge.*
179 Given the decline in the number of gB-specific CD8 T cells in the CVT combined with their shift
180 towards CD103 and granzyme B expression, we next evaluated how this affected the immune
181 response to vaginal HSV-2 challenge. We considered that the most rapid antiviral responses
182 would likely be mediated by tissue-resident gB-specific CD8 T cells, while circulating gB-specific
183 CD8 T cells would contribute to later responses. We challenged immunized mice at either 1mo
184 ("Early Memory") or 4mo ("Late Memory") after immunization (**Fig. 6A**). A similar proportion of
185 mice in each group survived lethal challenge (**Fig. 6B**), demonstrating that gB-specific memory
186 CD8 T cells were sufficient to confer protection against vaginal HSV-2 challenge in a subset of
187 immunized mice. However, mice challenged earlier after immunization began to show evidence
188 of faster viral clearance starting as early as 3.5d after challenge (**Fig. 6C**) and underwent
189 greater T cell expansion in the first 2.5d after challenge (**Fig. 6D**). We hypothesized that this
190 was due to quantitative and qualitative differences between the early and late CD8 T cell
191 compartment in the CVT. To better understand the relationship between CVT gB-specific CD8 T
192 cells and viral control, we used the mathematical model in **Equation 1** to characterize the

193 different gB-specific T cell response kinetics between the early and late memory groups. In this
194 model, susceptible cells in the CVT are infected by free HSV-2 virus, allowing them to produce
195 new virus or be killed by HSV-specific CD8 T cells (**Fig. 6E**, see methods for details). We
196 performed 100 model-fit rounds to all observations simultaneously for each group for both CVT
197 gB-specific CD8 T cell counts and viral load and overlaid these predictions onto our
198 experimental data (**Fig. 6D)**. In naive mice, gB-specific CD8 T cells were absent from or rare in
199 the CVT at 0-3.5d after challenge but were abundant by 6.5d after challenge (**Fig. 6D**, top left),
200 corresponding with the entry of primary effector T cells into the CVT. In mice challenged at
201 either early or late time points, gB-specific CD8 T cells increased dramatically in number
202 between 0d and 2.5d after HSV-2 infection and HSV viral titer fell by 6.5 post-challenge (**Fig.**
203 **6D**). The best model fits predicted that naive mice had the highest basic reproductive number,
204 meaning that they had the highest number of new cellular infections predicted to derive from a
205 single HSV-infected cell in a susceptible pool (**Fig. 6F**). In addition, the greater areas under
206 fitted gB tet^{+} T cell curves (shown in **Fig. 6D**, top row) were associated with earlier viral
207 clearance (**Fig. 6G**). These data suggest that the numerical and phenotypical changes we
208 observed within the CVT memory T cell compartment led to a decrease in the efficacy of the
209 anti-viral response in the first days after challenge. This may be of particular relevance to the
210 success of a vaccine-induced memory T cell response within the CVT, as the host-pathogen
211 events occurring within this early window likely result in the ultimate success or failure of the
212 protective response (25).

213 **Discussion**

214 Here, we report that immunization with LM-gB induces a robust HSV-specific memory
215 CD8 T cell population in both lymphoid and non-lymphoid tissues including the CVT. Over the
216 course of 5 months following immunization, gB-specific memory CD8 T cells in the CVT
217 numerically declined and gradually acquired expression of CD103 and granzyme B. Conversely,
218 HSV-specific CD8 T cells that were circulating (spleen, LN) or resident in the SI were
219 numerically and phenotypically stable over the same time course (**Figs. 1-3**). Previous studies
220 have shown that the memory CD8 T cell pool in the lung also declines over time (26-28).
221 However, around 90% of memory CD8 T cells in the lung are pulmonary vasculature-associated
222 (29), and are thus i.v. label positive, whereas about 90% of the memory CD8 T cells in the CVT
223 were i.v. label negative cells associated with the tissue parenchyma (**Fig. 2**). Thus, our data
224 suggest that memory CD8 T cell maintenance and differentiation in the CVT is directly regulated
225 by the tissue environment.

226 The cervicovaginal mucosa is distinct from other parts of the female reproductive tract
227 and other mucosal tissues in terms of epithelium type and physiology. Specifically, the vagina
228 and ectocervix are composed of type II mucosa and the endocervix and uterus are composed of
229 type I mucosa, with the cervical transformation zone marking the area where the simple
230 columnar epithelial cells of the endocervix meet the stratified squamous epithelial cells of the
231 ectocervix and vagina. In contrast, the gut and the lung, other mucosal tissues commonly
232 studied in the case of CD8 T cell memory, are type I mucosal surfaces (30). In addition to these
233 differences in the structure of the epithelium, there are differences in the complexity and
234 makeup of the microbiota at different mucosal tissue sites, which may also contribute to tissue-
235 specific environmental differences that could affect memory CD8 T cell differentiation and
236 function. In line with these differences between the vagina and mucosal tissues such as the gut,
237 a possible explanation for the observed delay in canonical resident-memory differentiation is

238 that the CVT tissue microenvironment is deficient in signals that are important for resident-
239 memory formation and maintenance (31).
240 Memory T cell frequencies in the blood are often still considered to be representative of
241 tissues and are used as a benchmark in clinical studies to assess immune responses to
242 vaccines and to establish correlates of protection. Our data indicate that there is a disconnect
243 between memory CD8 T cell frequency, phenotype, and stability in the periphery and the CVT.
244 The numerical and phenotypical changes of the memory CD8 T cell compartment 1 month vs. 5
245 months post-immunization ultimately influenced the rapidity of the immune response to vaginal
246 viral challenge (**Fig. 6**). These data highlight the importance of tissue-resident memory CD8 T
247 cells in mediating immunity in the CVT as well the need to study immune responses directly
248 within the relevant tissue.
249 Sexually-transmitted infections (STI) have a significant impact on global health, yet we
250 currently lack effective vaccines to prevent the majority of these infections, including HIV, HSV,
251 and bacterial STIs. Our data demonstrate that following systemic immunization, animals were
252 partially protected against HSV-2 lethality by gB-specific memory CD8 T cells (**Fig. 6**). This
253 protection was observed despite the lack of HSV-specific CD4 T or B cell memory, elements of
254 the immune response that are often considered crucial for protection against HSV-2 (32-35). It
255 is possible that a new focus on vaccine strategies that elicit memory CD8 T cells within the
256 genital mucosa, the site of first exposure to STIs, will increase vaccine efficacy. Design of these
257 approaches relies on understanding how memory CD8 T cells are maintained within these
258 genital tract mucosal tissues. Of note, our data from human vaginal tissue biopsies suggest that
259 the phenotype we observed in the mouse CVT is not specific to the mouse. Further studies are
260 required to better understand the relationship between the different subsets in human tissues as
261 well as their potential to self-renew.

262 In summary, we demonstrate that residence within cervicovaginal tissue alters memory
263 CD8 T cell differentiation and maintenance compared to circulating memory T cells (spleen, LN)
264 as well as tissue-resident memory T cells in the SI. Given that memory CD8 T cells in our study
265 were elicited by systemic immunization and *Listeria monocytogenes* is cleared from spleen and
266 liver within 7-8 days and antigen-presentation is short-lived in this context (36), our data support
267 the conclusion that the CVT tissue environment directly affects memory CD8 T cell
268 differentiation, leading to a steady decline in the antigen-specific memory CD8 T cell population
269 and concomitant phenotypic changes.
270

271 **Methods**

272 *Mice*

273 C57BL/6J (strain 000664) and B6.PL-*Thy1*^{a}/CyJ (strain 000406) mice were purchased from The
274 Jackson Laboratory and maintained in specific pathogen-free conditions at the Fred Hutchinson
275 Cancer Research Center (FHCRC). CD45.1 gBT-I$^{Tg/Tg}$ sires were crossed to B6.PL-*Thy1*^{a}/CyJ
276 dams to generate CD45.1/2 Thy1.1/2 gBT-I$^{Tg/0}$ mice for adoptive transfer experiments. All mice
277 used in experiments were female and were 8–30 weeks of age. Experiments were approved by
278 the Fred Hutchinson Cancer Research Center (FHCRC) Institutional Animal Care and Use
279 Committee.

280

281 *Study population*

282 Five women were recruited for this study and consented to vaginal biopsy and blood sampling.
283 Eligibility criteria included aged > 18 to < 45, assigned female sex at birth, in good general
284 health, normal PAP smear within the past 3-5 years, not menopausal, Hepatitis C negative and
285 no report of active genital tract irritation or infection. Additionally, participants were screened to
286 be negative for HIV, HSV-2, bacterial vaginosis, chlamydia, gonorrhea, and trichomonas
287 vaginalis. Subjects were not using any type of steroid or medication for treatment of
288 autoimmune disorders. Samples were not collected during menses. Informed written consent
289 was obtained from all participants. The study and procedures were approved by the FHCRC
290 Institutional Review Board.

291

292 *Adoptive CD8 T cell transfers*

293 CD44^{low} CD8 T cells were purified from spleen and lymph nodes of female CD45.1/2
294 Thy1.1/2 gBT-I$^{Tg/0}$ mice by negative selection using mouse CD8a^{+} T Cell Isolation kits (Miltenyi)
295 according to the manufacturer's protocol with some modifications. Specifically, spleens and
296 lymph nodes were dissociated by mashing through a 70 um cell filter. Cell suspensions were

297 incubated in ACK lysis buffer for 5 min. After red blood cell lysis, 10^8 cells were combined with
298 100 ul CD8 biotin antibody cocktail, 1 ul anti-CD44-biotin antibody (Clone IM7, eBioscience)
299 (37), and 400 ul cold culture media After 10 min incubation at 4C, 200 ul anti-biotin microbeads
300 and 300 ul cold culture media were added to the sample. After a further 15 min incubation at
301 4C, the sample was washed in 10 ml culture media, resuspended in 500 ul culture media, and
302 passed through an LS column (Miltenyi) on a MACS Separator magnet (Miltenyi). After washing
303 the column, the resulting suspension of purified CD8 T cells was diluted to 2.5×10^5 cells/ml in
304 sterile PBS. 5×10^4 cells were injected into recipient B6 mice via i.v. injection into the tail vein.
305 Purity and $CD44^-$ phenotype of the isolated CD8 T cell suspension was confirmed by flow
306 cytometry.
307
308 *Listeria monocytogenes immunization*
309 A strain of *Listeria monocytogenes* (LM) was generated to recombinantly express and
310 secrete ovalbumin containing the HSV-2 glycoprotein B-derived peptide SSIEFARL according to
311 previously described methods. Briefly, a pPL2 vector (38) containing ovalbumin (AA134–387)
312 (39) was digested with SapI. An oligonucleotide encoding SSIEFARL plus an alanine on each
313 side was ligated into the SapI restriction site. This construct was inserted into wildtype 10403s
314 LM by *E. coli* conjugation as previously described (38). The resulting SSIEFARL-expressing LM
315 strain (LM-gB) was grown in brain heart infusion broth to log phase. Bacterial concentration was
316 determined by measuring the optical density at 600 nm. Stocks were diluted to 2×10^4 CFU per
317 ml in sterile PBS before immunization. Naive B6 mice received 4,000 CFU i.v. via tail vein
318 injection. Infectious dose was confirmed by plating on brain-heart infusion media plates and
319 enumerating colonies.
320
321 *Herpes simplex virus type 2 infections and vaginal washes*

322 Mice were injected subcutaneously with 2 mg of medroxyprogesterone acetate
323 (Greenstone). Seven days later, mucus was removed from the vagina with a calcium alginate-
324 tipped swab (Puritan) and mice were infected via micropipette by applying 2×10^4 plaque-
325 forming units of wildtype herpes simplex virus type 2 (HSV-2) strain 186 syn+ to the vaginal
326 canal in a 10 ul volume (40, 41). To determine viral titer in the vaginal lumen, vaginal washes
327 were collected from mice by swabbing the vaginal canal, washing the vaginal canal with 50 uL
328 of titration buffer (PBS supplemented with 100 ug/ml $MgCl_2$, 132 ug/ml $CaCl_2$, 10 mg/ml
329 glucose, and 1% FBS) and repeating swabbing of the vaginal canal. Both swabs and the 50 ul
330 of wash buffer were added to 950 ul of cold titration buffer and stored at -80C until analysis.
331 Viral titer was determined by plaque assay on Vero cells (ATCC). Stock solutions of HSV-2
332 were propagated on Vero cells and titered by plaque assay to verify infectious doses. After
333 infection with HSV-2, mice were monitored daily and clinical disease progression was scored as
334 previously described (33) with minor modification. Scores were defined as follows: 0, No sign; 1,
335 slight genital erythema; 2, moderate genital erythema and edema; 3, significant genital
336 inflammation with visible lesion; 4, hind leg paralysis or other severe condition requiring
337 euthanasia; 5, moribund or dead. Mice were euthanized if they were moribund or showed signs
338 of severe disease, including hind leg weakness, hind leg paralysis, or hunched posture.
339
340 *Labeling of T cells in the vasculature*
341 To discriminate CD8 T cells in the vasculature from those located within tissues, we
342 utilized an intravascular labeling technique as previously described (18). Briefly, mice were
343 injected i.v. with 3 ug anti-CD8b antibody conjugated to either FITC or APC (Clone: H35-17.2,
344 eBioscience) in PBS via the tail vein 2-5 min before euthanasia by CO_2 inhalation.
345
346 *Tissue collection and processing*

347 Mouse

348 Blood samples were collected from live mice by submandibular venipuncture or via
349 thoracic venipuncture after sacrifice. Spleens and CVT-draining iliac and inguinal lymph nodes
350 were dissociated by mashing through 70 um cell filters. For spleen and blood samples, red
351 blood cells were lysed by incubating in ACK lysis buffer for 5-20 min.

352 Murine cervicovaginal tracts (consisting of the vagina, ectocervix, and endocervix) were
353 dissected by removing the bladder and excising the region between the vaginal opening and the
354 uterine corpus. To prepare single cell suspensions from cervicovaginal tracts, tissues were
355 minced with scissors and then incubated in 2 ml DMEM medium supplemented with 2% FBS, 2
356 mg/ml collagenase D, and 1.5 mg/ml DNase I (Roche) for 30 minutes at 37C with gentle
357 rocking. Tissues were then re-suspended in HBSS supplemented with EDTA and 2% FBS and
358 incubated for 5 minutes at 37 degrees C to quench the collagenase reaction. Finally, tissues
359 were dissociated by mashing through 70 um filters.

360 Single cell suspensions were prepared from small intestines by removing the Peyer's
361 patches and mesentery, washing thoroughly with HBSS supplemented with 2% FBS, and
362 incubating in 25 ml HBSS with 2% FBS, 5 mM EDTA, and 1 mM dithiothreitol for 15 min at 37C
363 with gentle rocking. Then, tissue pieces were washed and incubated in 5 ml DMEM medium
364 supplemented with 2% FBS, 2 mg/ml collagenase D, and 1.5 mg/ml DNase I (Roche, Basel,
365 Switzerland) for 30 minutes at 37C with gentle rocking. Finally, samples were passed through
366 19g needles and mashed through 70 um filters.

367

368 Human

369 Blood was collected into acid citrate dextrose tubes and mixed. Tubes were spun at 1000 xg for
370 10 minutes to remove the plasma. The remaining blood was diluted 1:2 in PBS and layered on a
371 Lymphoprep (STEMCELL) gradient and centrifuged at 800 xg for 20 minutes. The PBMC layer
372 was then removed and washed with PBS. Tissues were transported from the clinic in ice cold

373 PBS and immediately processed upon arrival. Biopsy samples were trimmed to $2mm^2$ pieces
374 and digested with collagenase II (700 units/ml, Sigma-Aldrich) and DNAse I (1unit/ml, Sigma-
375 Aldrich) for two subsequent 30 minute-digestions at 37°C as previously described (42). Single
376 cell suspensions were then washed and filtered before use.
377
378 *Generation of H-2Kb tetramers*
379 Biotinylated H-2Kb monomers containing HSV-2 gB SSIEFARL were generated by the
380 FHCRC Immune Monitoring Lab. Tetramers were generated by incubating monomers with
381 premium-grade streptavidin-APC or streptavidin-PE (Invitrogen) at a 4:1 molar ratio for 30
382 minutes at room temperature.
383
384 *Cell Staining for Flow Cytometry and Sorting*
385 Cells were incubated in LIVE/DEAD fixable amine-reactive viability dye (Invitrogen),
386 blocked for Fc binding (Clone 2.4G2 for mice or TruStain (BioLegend) for human), and then
387 stained with tetramers and antibodies.
388 The following fluorochrome-conjugated antibodies were used to stain mouse cells for
389 flow cytometry: anti-CD8 (Clone 53-6.7, PerCP-eFluor710), anti-CD4 (Clone GK1.5, APC-
390 eFluor780), anti-CD45.1 (Clone A20, Brilliant Ultraviolet 395), anti-CD45.2 (Clone 104, Brilliant
391 Ultraviolet 737), anti-Thy1.1 (Clone HIS51, FITC or SuperBright645), anti-CD44 (Clone IM7,
392 APC or AlexaFluor700), anti-CD69 (Clone H1.2F3, PE-Dazzle594 or PE-Cy7), anti-CD103
393 (Clone M290, Brilliant Violet 786), anti-granzyme B (Clone GB11, Pacific Blue), and anti-TCF-1
394 (Clone C63D9, PE). Anti-CD8, anti-CD4, and anti-Thy1.1 were purchased from eBioscience.
395 Anti-CD45.1, anti-CD45.2, anti-CD44, and anti-CD103 were purchased from BD. Anti-CD69 and
396 anti-granzyme B antibodies were purchased from Biolegend. Anti-TCF-1 antibody was
397 purchased from Cell Signaling Technologies.

398 The following fluorochrome-conjugated antibodies were used to stain human cells for
399 flow cytometry: anti-CD3 (Clone UCHT1, Brilliant Ultraviolet 661), anti-CD45 (Clone HI30,
400 Brilliant Ultraviolet 805), anti-CD8 (Clone RPA-T8, Brilliant Ultraviolet 496), anti-CD4 (Clone
401 RPA-T4, Brilliant Violet 605), anti-CD45RA (Clone Clone HI100, APC-H7), anti-granzyme B
402 (Clone GB11, AlexaFluor700), anti-CD103 (Clone Ber-ACT8, Brilliant Violet 750), and anti-TCF-
403 1 (Clone C63D9, PE). Anti-CD3, anti-CD45, anti-CD4, anti-CD8, anti-CD45RA, anti-CD103, and
404 anti-Granzyme B were purchased from BD. Anti-TCF-1 antibody was purchased from Cell
405 Signaling Technologies.
406
407 Intracellular staining was conducted after fixation and membrane permeabilization using
408 Cytofix/Cytoperm Fixation/Permeabilization Kits (BD). If TCF-1 was included in the staining
409 panel, intracellular staining was conducted after nuclear permeabilization using
410 Foxp3/Transcription Factor Staining Kits (eBioscience) according to the manufacturer's protocol.
411 Samples were acquired on a FACSymphony instrument (BD) or sorted on a FACSAria (BD). To
412 estimate cell counts, 2×10^5 AccuCheck Counting Beads (ThermoFisher) were added to each
413 sample immediately before acquisition.
414
415 *Single Cell RNA Sequencing and Data Analysis*
416 In order to generate single cell transcriptomic data, CD8 T cell populations of interest
417 were sorted using a FACSAriaII fitted with a 70 um nozzle (BD). Live CD45.2$^+$ CD8a$^+$ CD8b i.v.-
418 label$^+$ cells from the blood and live CD45.2$^+$ CD8a$^+$ CD8b i.v.-label$^-$ cells from the CVT were
419 sorted and loaded onto a Chromium Controller (10x Genomics) to generate gel beads in
420 emulsion. After cDNA synthesis, samples were further processed using the Chromium Single
421 Cell 3' RNA sequencing kit version 2 (10x Genomics) and the resulting libraries were
422 sequenced on a HiSeq 2500 Next Generation Sequencer (Illumina) at the FHCRC Genomics
423 Shared Resource Facility. Cell Ranger software (10x Genomics) was used to generate FASTQ

424 files, demultiplex samples, and count transcripts per cell. The processed data were analyzed
425 using R (R Development Core Team) and the package Seurat version 2.3.4 (43). Quality
426 filtering steps included removal of genes detected in fewer than three cells and removal of cells
427 in which fewer than 200 genes were detected or in which greater than 5% of detected genes
428 were mitochondrial. Count data were normalized for each gene by dividing the per-cell
429 expression count by the total counts of all genes summed for that cell, multiplying the resulting
430 value by 10,000, adding 1, and taking the natural log. Variable genes were identified on the
431 basis of having a mean of non-zero expression values between 0.0125 and 3 and a standard
432 deviation of all expression values greater than 0.5. Data were scaled and centered using a
433 linear model that adjusted for the number of unique molecular identifiers per cell and the percent
434 mitochondrial genes detected per cell. Principle components analysis was performed using the
435 scaled and normalized data for all variable genes, and the first 20 principle components were
436 used to compute and display uniform manifold approximation and projection (UMAP) (44) plots
437 and to cluster the data using a graph-based clustering algorithm (45) implemented in Seurat.
438 Contaminating non-T cell subsets were identified by graph-based clustering and removed based
439 on high expression of *Krt4*, *Krt19*, *Cd74*, *Cd79a*, and *Cd79b* and no expression of *Cd3e*. Genes
440 that were differentially expressed between specific populations or clusters of cells were
441 identified using model-based analysis of single cell transcriptomics (MAST) (46) using criteria
442 described in results and in figure legends.
443
444 *Statistical Analysis*
445 Sample means between two unpaired groups were compared by *t*-test. Sample means
446 between three or more unpaired groups were compared by ordinary one-way ANOVA with
447 Tukey's multiple comparisons test. Sample means between three paired groups were compared
448 by repeated measures ANOVA with Greenhouse-Geisser correction. Paired mean fluorescence

intensity or relative frequency data were analyzed via paired *t*-test. All cell count and viral titer data were $\log_{10}$-transformed before graphing and analysis. Error bars represent standard deviations. Exact *P*-values are given for all results where $P < 0.05$. Analysis was performed using Prism 7 (GraphPad Software).

HSV-2 and CD8 T cell Dynamics Modeling

To understand the virus and gB-specific CD8 T cell dynamic differences between the Naive, Early Memory, and Late Memory groups as reflected in the observations, we used an acute viral infection model that includes a cytotoxic effect of the CD8 T cell compartment. In this model, susceptible cells (S) are infected at rate βVS by free HSV-2 virus (V). Productively HSV-2-infected cells (I) have a clearance that is intrinsic or mediated by a humoral response with rate $\delta_I I$ or a clearance mediated by HSV-specific CD8 T cells (E) with killing rate kEI. Free virus is produced at a rate pI and cleared at rate cV. HSV-specific CD8 T cells are cleared at rate $\delta_E E$ and proliferate in the presence of infected cells at a maximum rate ωEI. We also assumed the proliferation of HSV-specific CD8 T cells is constrained when infected and effector cells grow over saturation levels I_{50} and E_{50}, respectively. Under these assumptions the model has the form (see schematics in **Fig. 6D**):

$$\begin{aligned} \frac{dS}{dt} &= -\beta VS \\ \frac{dI}{dt} &= \beta VS - \delta_I I - kEI \\ \frac{dV}{dt} &= pI - cV \\ \frac{dE}{dt} &= \frac{\omega EI}{\left(1+\frac{I}{I_{50}}\right)\left(1+\frac{E}{E_{50}}\right)} - \delta_E E. \end{aligned} \qquad \textbf{(1)}$$

The basic reproductive ratio, R_0, which represents the number of secondary infections produced by an HSV-infected cell when introduced into a susceptible population, was calculated as $R_0 = \frac{\beta p T_0}{c(\delta_I + kE_0)}$. When $R_0 < 1$, viremia is controlled.

470 Due to the limitation that some data points were from individual mice rather than
471 repeated from the same mouse across all time points, we fit the solution of the model for *V* and
472 *E* to the absolute viral load genome copies per vaginal wash and HSV-specific CD8 T cell
473 counts in CVT from all animals in each group. In this way, given that there were several
474 observations for each timepoint, we performed 100 rounds of model fits to observations from all
475 individual animals for each group with different initial parameter guesses in the optimization
476 algorithm. We assumed that all outcomes from the 100 fit rounds were plausible predictions of
477 the data and represented the variability in the infection dynamics in each group. For each round,
478 we re-parameterized the model in function of R_0, and used a nonlinear least-squares approach
479 using the differential evolution and the L-BFGS-B algorithms in R (R Development Core
480 Team) to fit the model and to estimate parameters: V_0, pT_0, E_0, R_0, δ, c, k, ω, δ_E, I_{50} and E_{50}.
481 Since mice were inoculated with ~2.3×10^6 HSV genomes, we set that number as the upper limit
482 for V_0. We also constrained the value estimate E_0 to the maximum and minimum HSV-specific
483 CD8 T cell observations at the moment of virus challenge. Finally, we ensured that $R_0 > 1$ in all
484 fitting rounds. In all simulations $t = 0$ represented the time of the HSV-2 vaginal challenge.
485 From the best fits, we computed the predicted time of viral clearance as the time when viral load
486 crossed the detection limit for the PCR assay of 4615.4 genomes per vaginal wash. We also
487 computed the predicted area under the curve of HSV-specific CD8 T cells using best fits of
488 variable *E* from challenge until the time of viral clearance.
489 We repeated the fits by exploring different possibilities for constraining HSV-specific
490 CD8 T cell growth. Specifically, we explored a model were CD8 growth is constrained only by a
491 saturation level in HSV-infected cells, i.e. $\frac{dE}{dt} = \frac{\omega EI}{\left(1+\frac{I}{I_{50}}\right)} - \delta_E E$, or only by a saturation for the
492 number of effector cells, i.e. $\frac{dE}{dt} = \frac{\omega EI}{\left(1+\frac{E}{E_{50}}\right)} - \delta_E E$. To determine the best and most parsimonious
493 model, we computed the Akaike Information Criteria, $AIC = n \ln \overline{SSE} + 2m$, where *m* is the

494 number of parameters estimated, *n* the number of data points in each group and $\overline{SSE}$ is the
495 average sum of squares error of all the 100 model-fit rounds in each group. We assumed a
496 model had similar support from the data if the difference between its AIC and the best model
497 (lowest) AIC was less than two. We selected and showed results from the model with the lowest
498 AIC.
499
500 **Abbreviations**
501 AIC, Akaike information criteria
502 AUC, area under curve
503 CVT, cervicovaginal tissue
504 dLN, CVT-draining lymph nodes
505 gB, HSV glycoprotein B
506 LM-gB, *Listeria monocytogenes* strain expressing the SSIEFARL peptide from HSV glycoprotein
507 B
508 LN, lymph node
509 SI, small intestine
510 SI LP, small intestine lamina propria

Acknowledgements

We thank Kristin Weakly for excellent technical assistance. This work was supported by NIH grants R01 AI123323 (MP), R01 AI121129 to (JTS, JML and MP), R01 AI131914 (JML), R01 AI141435 (JML), T32 AI07140 and the Doug and Maggie Walker Fellowship (ASWD), and T32 AI007509 and F31 AI140514 (VD). FM is an ISAC scholar.

517 **References**

518 1. Pattacini L, Woodward Davis A, Czartoski J, Mair F, Presnell S, Hughes SM, et al. A pro-
519 inflammatory CD8+ T-cell subset patrols the cervicovaginal tract. *Mucosal immunology.*
520 2019.
521 2. Kumar BV, Kratchmarov R, Miron M, Carpenter DJ, Senda T, Lerner H, et al. Functional
522 heterogeneity of human tissue-resident memory T cells based on dye efflux capacities.
523 *JCI insight.* 2018;3(22).
524 3. Kumar BV, Ma W, Miron M, Granot T, Guyer RS, Carpenter DJ, et al. Human Tissue-
525 Resident Memory T Cells Are Defined by Core Transcriptional and Functional
526 Signatures in Lymphoid and Mucosal Sites. *Cell Rep.* 2017;20(12):2921-34.
527 4. Watanabe R, Gehad A, Yang C, Scott LL, Teague JE, Schlapbach C, et al. Human skin
528 is protected by four functionally and phenotypically discrete populations of resident and
529 recirculating memory T cells. *Science translational medicine.* 2015;7(279):279ra39.
530 5. Gebhardt T, Wakim LM, Eidsmo L, Reading PC, Heath WR, and Carbone FR. Memory T
531 cells in nonlymphoid tissue that provide enhanced local immunity during infection with
532 herpes simplex virus. *Nat Immunol.* 2009;10(5):524-30.
533 6. Mackay LK, Stock AT, Ma JZ, Jones CM, Kent SJ, Mueller SN, et al. Long-lived
534 epithelial immunity by tissue-resident memory T (TRM) cells in the absence of persisting
535 local antigen presentation. *Proceedings of the National Academy of Sciences of the*
536 *United States of America.* 2012;109(18):7037-42.
537 7. Sathaliyawala T, Kubota M, Yudanin N, Turner D, Camp P, Thome JJ, et al. Distribution
538 and compartmentalization of human circulating and tissue-resident memory T cell
539 subsets. *Immunity.* 2013;38(1):187-97.
540 8. Schenkel JM, Fraser KA, Vezys V, and Masopust D. Sensing and alarm function of
541 resident memory CD8(+) T cells. *Nat Immunol.* 2013;14(5):509-13.

542 9. Shin H, and Iwasaki A. Tissue-resident memory T cells. *Immunol Rev.* 2013;255(1):165-
543 81.
544 10. Wakim LM, Woodward-Davis A, and Bevan MJ. Memory T cells persisting within the
545 brain after local infection show functional adaptations to their tissue of residence.
546 *Proceedings of the National Academy of Sciences of the United States of America.*
547 2010;107(42):17872-9.
548 11. Milner JJ, Toma C, Yu B, Zhang K, Omilusik K, Phan AT, et al. Runx3 programs CD8(+)
549 T cell residency in non-lymphoid tissues and tumours. *Nature.* 2017;552(7684):253-7.
550 12. Milner JJ, and Goldrath AW. Transcriptional programming of tissue-resident memory
551 CD8(+) T cells. *Curr Opin Immunol.* 2018;51:162-9.
552 13. Schenkel JM, and Masopust D. Tissue-resident memory T cells. *Immunity.*
553 2014;41(6):886-97.
554 14. Masopust D, and Soerens AG. Tissue-Resident T Cells and Other Resident Leukocytes.
555 *Annu Rev Immunol.* 2019;37:521-46.
556 15. Szabo PA, Miron M, and Farber DL. Location, location, location: Tissue resident memory
557 T cells in mice and humans. *Sci Immunol.* 2019;4(34).
558 16. Becker M, Levings MK, and Daniel C. Adipose-tissue regulatory T cells: Critical players
559 in adipose-immune crosstalk. *Eur J Immunol.* 2017;47(11):1867-74.
560 17. Anderson KG, Mayer-Barber K, Sung H, Beura L, James BR, Taylor JJ, et al.
561 Intravascular staining for discrimination of vascular and tissue leukocytes. *Nat Protoc.*
562 2014;9(1):209-22.
563 18. Galkina E, Thatte J, Dabak V, Williams MB, Ley K, and Braciale TJ. Preferential
564 migration of effector CD8+ T cells into the interstitium of the normal lung. *J Clin Invest.*
565 2005;115(12):3473-83.
566 19. Gibbs A, Buggert M, Edfeldt G, Ranefall P, Introini A, Cheuk S, et al. Human
567 Immunodeficiency Virus-Infected Women Have High Numbers of CD103-CD8+ T Cells

568 Residing Close to the Basal Membrane of the Ectocervical Epithelium. *The Journal of*
569 *infectious diseases.* 2018;218(3):453-65.
570 20. Steinert EM, Schenkel JM, Fraser KA, Beura LK, Manlove LS, Igyarto BZ, et al.
571 Quantifying Memory CD8 T Cells Reveals Regionalization of Immunosurveillance. *Cell.*
572 2015;161(4):737-49.
573 21. Casey KA, Fraser KA, Schenkel JM, Moran A, Abt MC, Beura LK, et al. Antigen-
574 independent differentiation and maintenance of effector-like resident memory T cells in
575 tissues. *Journal of immunology (Baltimore, Md : 1950).* 2012;188(10):4866-75.
576 22. Masopust D, Vezys V, Wherry EJ, Barber DL, and Ahmed R. Cutting edge: gut
577 microenvironment promotes differentiation of a unique memory CD8 T cell population.
578 *Journal of immunology (Baltimore, Md : 1950).* 2006;176(4):2079-83.
579 23. Sarkar S, Teichgraber V, Kalia V, Polley A, Masopust D, Harrington LE, et al. Strength of
580 stimulus and clonal competition impact the rate of memory CD8 T cell differentiation.
581 *Journal of immunology (Baltimore, Md : 1950).* 2007;179(10):6704-14.
582 24. Zhou X, Yu S, Zhao DM, Harty JT, Badovinac VP, and Xue HH. Differentiation and
583 persistence of memory CD8(+) T cells depend on T cell factor 1. *Immunity.*
584 2010;33(2):229-40.
585 25. Haase AT. Targeting early infection to prevent HIV-1 mucosal transmission. *Nature.*
586 2010;464(7286):217-23.
587 26. Kohlmeier JE, and Woodland DL. Memory T cell recruitment to the lung airways. *Curr*
588 *Opin Immunol.* 2006;18(3):357-62.
589 27. Ely KH, Cookenham T, Roberts AD, and Woodland DL. Memory T cell populations in the
590 lung airways are maintained by continual recruitment. *Journal of immunology (Baltimore,*
591 *Md : 1950).* 2006;176(1):537-43.

592 28. Zammit DJ, Turner DL, Klonowski KD, Lefrancois L, and Cauley LS. Residual antigen
593 presentation after influenza virus infection affects CD8 T cell activation and migration.
594 *Immunity.* 2006;24(4):439-49.
595 29. Anderson KG, Sung H, Skon CN, Lefrancois L, Deisinger A, Vezys V, et al. Cutting
596 edge: intravascular staining redefines lung CD8 T cell responses. *Journal of immunology*
597 *(Baltimore, Md : 1950).* 2012;189(6):2702-6.
598 30. Iwasaki A. Antiviral immune responses in the genital tract: clues for vaccines. *Nat Rev*
599 *Immunol.* 2010;10(10):699-711.
600 31. Liu Y, Ma C, and Zhang N. Tissue-Specific Control of Tissue-Resident Memory T Cells.
601 *Crit Rev Immunol.* 2018;38(2):79-103.
602 32. Milligan GN, Bernstein DI, and Bourne N. T lymphocytes are required for protection of
603 the vaginal mucosae and sensory ganglia of immune mice against reinfection with
604 herpes simplex virus type 2. *Journal of immunology (Baltimore, Md : 1950).*
605 1998;160(12):6093-100.
606 33. Morrison LA, Da Costa XJ, and Knipe DM. Influence of mucosal and parenteral
607 immunization with a replication-defective mutant of HSV-2 on immune responses and
608 protection from genital challenge. *Virology.* 1998;243(1):178-87.
609 34. Dudley KL, Bourne N, and Milligan GN. Immune protection against HSV-2 in B-cell-
610 deficient mice. *Virology.* 2000;270(2):454-63.
611 35. Petro CD, Weinrick B, Khajoueinejad N, Burn C, Sellers R, Jacobs WR, Jr., et al. HSV-2
612 DeltagD elicits FcgammaR-effector antibodies that protect against clinical isolates. *JCI*
613 *insight.* 2016;1(12).
614 36. Turner DL, Cauley LS, Khanna KM, and Lefrancois L. Persistent antigen presentation
615 after acute vesicular stomatitis virus infection. *J Virol.* 2007;81(4):2039-46.

616 37. Prlic M, Blazar BR, Khoruts A, Zell T, and Jameson SC. Homeostatic expansion occurs
617 independently of costimulatory signals. *Journal of immunology (Baltimore, Md : 1950).*
618 2001;167(10):5664-8.
619 38. Lauer P, Chow MY, Loessner MJ, Portnoy DA, and Calendar R. Construction,
620 characterization, and use of two Listeria monocytogenes site-specific phage integration
621 vectors. *Journal of bacteriology.* 2002;184(15):4177-86.
622 39. Zehn D, Lee SY, and Bevan MJ. Complete but curtailed T-cell response to very low-
623 affinity antigen. *Nature.* 2009;458(7235):211-4.
624 40. Parr MB, Kepple L, McDermott MR, Drew MD, Bozzola JJ, and Parr EL. A mouse model
625 for studies of mucosal immunity to vaginal infection by herpes simplex virus type 2.
626 *Laboratory investigation; a journal of technical methods and pathology.* 1994;70(3):369-
627 80.
628 41. Jones CA, Taylor TJ, and Knipe DM. Biological properties of herpes simplex virus 2
629 replication-defective mutant strains in a murine nasal infection model. *Virology.*
630 2000;278(1):137-50.
631 42. McKinnon LR, Hughes SM, De Rosa SC, Martinson JA, Plants J, Brady KE, et al.
632 Optimizing viable leukocyte sampling from the female genital tract for clinical trials: an
633 international multi-site study. *PLoS One.* 2014;9(1):e85675.
634 43. Butler A, Hoffman P, Smibert P, Papalexi E, and Satija R. Integrating single-cell
635 transcriptomic data across different conditions, technologies, and species. *Nature*
636 *biotechnology.* 2018;36(5):411-20.
637 44. McInnes L, Healy J, and Melville J. *arXiv e-prints*. 2018.
638 45. Waltman L, and van Eck NJJTEPJB. A smart local moving algorithm for large-scale
639 modularity-based community detection. 2013;86(11):471.

640 46. Finak G, McDavid A, Yajima M, Deng J, Gersuk V, Shalek AK, et al. MAST: a flexible
641 statistical framework for assessing transcriptional changes and characterizing
642 heterogeneity in single-cell RNA sequencing data. *Genome Biol.* 2015;16:278.
643

644 **Figure Legends**

645 **Figure 1. The cervicovaginal CD8 T cell memory compartment of LM-gB-immunized mice**
646 **is poorly maintained after immunization. (A)** Schematic of experiment to assess
647 maintenance of HSV-specific T cell compartment in lymphoid and mucosal tissues of immunized
648 mice. **(B)** HSV-specific cells were identified in the blood via staining with an H-2Kb SSIEFARL
649 tetramer conjugated to PE. Left, representative flow plots gated on CD8 T cells. Right, gB
650 tetramer$^+$ CD8 T cell abundance as a percentage of total blood CD8 T cells. **(C-D)** Number and
651 relative abundance of HSV-specific CD8 T cells in spleen, CVT-draining LN (dLN), small
652 intestine lamina propria (SI LP), and cervicovaginal tissue (CVT) 1mo and 5mo after LM-gB
653 immunization. Data in B, C, and D are pooled from 2-5 individual experiments. Each dot in B
654 (right) represents the mean value of 20 mice from a representative experiment. Each dot in C
655 and D represents an individual mouse. Error bars represent mean ± SD. *P*-values in D were
656 calculated via *t*-test using $\log_{10}$-transformed values. Exact *P*-values are given for all values <
657 0.05.

658

659 **Figure 2. Gradual changes occur within the CVT HSV-specific CD8 T cell compartment**
660 **that are not mirrored in other organs. (A)** Percentage of i.v. label$^-$ HSV-specific CD8 T cells
661 in different lymphoid and non-lymphoid tissues at 1mo, 3mo, and 5mo after immunization based
662 on gating shown in Fig. S1. **(B)** Representative staining showing CD69 and CD103 expression
663 on HSV-specific CD8 T cells in the CVT 1mo and 5mo after immunization. **(C)** Stacked bar plots
664 showing relative abundance of each of four subsets of HSV-specific CD8 T cells based on
665 CD69 and CD103 expression in the i.v. label$^+$ and i.v. label$^-$ fractions of the CVT and SI LP. **(D)**
666 CD103 expression on i.v. label$^-$ gB tetramer$^+$ CD8 T cells in the CVT 1mo, 3mo, and 5mo after
667 immunization. **(E)** Total count of each of four subsets of HSV-specific CD8 T cells based on
668 CD69 and CD103 expression 1mo, 3mo, and 5mo after immunization. Data in A, C, D, and E
669 are pooled from at least 2 individual experiments per time point. Data in B are from one

670 representative experiment. Each dot in A, D, and E represents an individual mouse. Error bars
671 represent mean ± SD. *P*-values in D and E were calculated via ordinary one-way ANOVA with
672 Tukey's post-hoc test using $\log_{10}$-transformed values for numbers and untransformed values for
673 percentages. Exact *P*-values are given for all values <0.05.
674
675 **Figure 3. The immunization-induced cervicovaginal-resident CD8 T cell compartment**
676 **acquires expression of granzyme B much later than the gut-resident CD8 T cell**
677 **compartment. (A)** Number of granzyme B-expressing cells among HSV-specific CD8 T cells at
678 time points after LM-gB immunization. **(B)** Frequency of granzyme B^+ cells among HSV-specific
679 CD8 T cells in spleen, dLN, CVT, and SI LP at 1mo, 3mo, and 5mo post-immunization. **(C)**
680 Concatenated flow files from 10 mice showing CD103 and granzyme B co-expression among
681 the HSV-specific CD8b i.v. $label^-$ populations in the CVT and dLN 5mo after LM-gB
682 immunization. **(D-E)** Frequency of CD69 and CD103 expression within granzyme B^+ HSV-
683 specific CD8 T cells in the CVT and SI LP 1mo, 3mo, and 5mo after immunization. Data in A-E
684 are pooled from at least 2 individual experiments. Each dot or triangle in A, B, and D represents
685 an individual mouse. Error bars represent mean ± SD. *P*-values in A and B were calculated via
686 ordinary one-way ANOVA with Tukey's post-hoc test using $\log_{10}$-transformed values for
687 numbers and untransformed values for percentages. Exact *P*-values are given for all values
688 <0.05.
689
690 **Figure 4. LM-gB induced memory CD8 T cells in blood and cervicovaginal tissue undergo**
691 **transcriptional changes between 1mo and 5mo after immunization. (A)** Schematic of
692 experimental design to evaluate single cell transcriptomes of HSV-specific and non-specific
693 CD8 T cells via droplet-based methodology. **(B-C)** Volcano plot of $\log_2$-transformed fold
694 changes and unadjusted *P*-values between Early and Late Memory HSV-specific CVT CD8 T

695 cells from (B) blood and (C) CVT. For the CVT plot, all genes with Bonferroni-adjusted *P*-values
696 <0.05 are labeled. For the blood plot, all genes with Bonferroni-adjusted *P*-values <0.05 and
697 log_2-transformed fold change >0.5 are labeled. Filled dots represent genes with Bonferroni-
698 adjusted *P*-values <0.05. Each dot in B represents averaged single cell fold change data for an
699 individual gene.
700
701 **Figure 5. Cervicovaginal-resident CD8 T cells lack expression of TCF-1 transcript and**
702 **protein. (A)** Protein expression of CD103 and TCF-1 among HSV-specific i.v. label$^-$ CD8 T cells
703 in CVT (red) or dLN (black) 1mo after LM-gB immunization. Flow plots represent concatenated
704 data from 5 mice. **(B)** TCF-1 median fluorescence intensity from CD103$^+$ or CD103$^-$ subsets of
705 HSV-specific CD8 T cells compared to lymph node (LN) in CVT 42 days after LM-gB
706 immunization. **(C)** Violin plots of normalized single cell *Tcf7* transcript expression level in sorted
707 gB tetramer$^+$ cells from blood and CVT from Early (1mo) and Late (7mo) time points after
708 immunization. **(D)** Representative flow plot of CD103 and TCF-1 among CD8 T cells in CVT
709 (red) or CD45RA$^-$ CD8 T cells in blood (black) from an HSV-negative participant. **(E)** TCF-1
710 median fluorescence intensity and frequency from CD103$^+$ or CD103$^-$ subsets of CD8 T cells
711 from the CVT compared to CD45RA$^-$ CD8 T cells in matched blood from five HSV-2-negative
712 women. **(F)** Representative flow plot of CD103 and granzyme B expression by CD8 T cells in
713 CVT from an HSV-negative participant. **(G)** Relative abundance of granzyme B expression
714 among CD103$^+$ CD8 T cells in CVT from five HSV-negative women. A-B represent data from
715 one representative experiment (n=3-5). C represents data from one experiment using pooled
716 mouse samples (n=9 per group). Data from E-G represent pooled results from study
717 participants (n=5). Each dot in B represents an individual mouse. Each dot in E and G
718 represents an individual participant. Error bars represent mean ± SD. *P*-values in B were
719 calculated via repeated measures ANOVA with Greenhouse-Geisser correction. *P*-values in F
720 were calculated via paired *t*-test. Exact *P*-values are given for all values <0.05.

721

722 **Figure 6. LM-gB immunized mice are protected against severe disease after lethal**
723 **intravaginal challenge with HSV-2, but the efficacy of the immune response wanes over**
724 **time. (A)** Experiment schematic to compare protective efficacy of LM-gB immunization 1mo and
725 4mo after administration. **(B)** LM-gB immunized or naive mice were treated with 2 mg
726 medroxyprogesterone s.c. and vaginally challenged with 10^4 pfu wildtype HSV-2 7d later.
727 Survival of naive mice and mice challenged at either the ”Early” or “Late” memory time point
728 after LM-gB immunization. **(C)** Vaginal washes were collected from infected mice in B at 2.5d,
729 3.5d, and 6.5d post-challenge. HSV-2 pfu per ml of vaginal wash was determined by plaque
730 assay on Vero cell monolayers and viral titers were compared between groups of challenged
731 mice at each time point. Pink dots represent mice that survived challenge, as shown in B. **(D)**
732 Top: number of HSV-specific CD8 T cells recovered from the CVT at each post-challenge time
733 point in Naive, Early Memory, and Late Memory mice, with modeling estimates of immune
734 response kinetics overlaid in blue. Bottom: HSV genomes recovered by PCR at each post-
735 challenge time point in Naive, Early Memory, and Late Memory mice, with modeling estimates
736 of viral expansion and control overlaid in blue. **(E)** Schematic of mathematical model used to
737 relate CVT-infiltrating CD8 T cell immune response to HSV-2 viral expansion kinetics. *S* and *I*
738 represent the number of susceptible and infected cells per CVT, respectively; *E*, the number of
739 gB tet^+ CD8 T cells per CVT; and *V* the number of HSV genomes per vaginal wash. **(F)** Model
740 estimates of basic reproductive ratios (number of new cells infected by one infected cell when
741 introduced into a pool of susceptible cells) for Naive, Early Memory, and Late Memory mice. **(G)**
742 Scatter plot of areas under curves (AUC) from D and corresponding predicted day of viral
743 clearance. Dotted line represents a fitted line from quadratic regression. Data in B, C, and D are
744 pooled from at least 2 individual experiments (n=8-14 per group in B). Each dot, square, or
745 triangle in B, C, and D represents data from an individual mouse. Each dot, square, or triangle
746 in F and G represents one model estimate. *P*-values in C were calculated via unpaired *t*-test

747 using $\log_{10}$-transformed values. *P*-values in F were calculated via pairwise corrected Mann-
748 Whitney's test using Bonferroni's correction. *P*- and r_s-value in G were calculated via
749 Spearman's rank correlation. Exact *P*-values are given for all values <0.05.
750
751 **Figure S1. Example of gating strategies used to identify CD8 T cells in mouse and human**
752 **CVT. (A)** Representative example from CVT of mouse sacrificed 1mo after LM-gB
753 immunization. **(B)** Representative example of T cell gating strategy from vaginal biopsies from
754 one study participant. **(C)** Comparison of intravascular staining using CD8b-APC in blood, dLN,
755 spleen, SI LP, and CVT. Representative staining examples from one mouse sacrificed 5mo after
756 LM-gB immunization.
757
758 **Figure S2. Comparison of TCF-1 protein expression in HSV-specific CD8 T cells from**
759 **mouse CVT and SI LP. (A)** Protein expression of CD103 and TCF-1 among HSV-specific i.v.
760 label$^-$ CD8 T cells in CVT, SI LP, and dLN 3mo after LM-gB immunization. Flow plots represent
761 concatenated data from 3 mice. **(B)** TCF-1 median fluorescence intensity from CD103$^+$ or
762 CD103$^-$ subsets of HSV-specific CD8 T cells from CVT and SI LP compared to LN 3mo after
763 immunization.

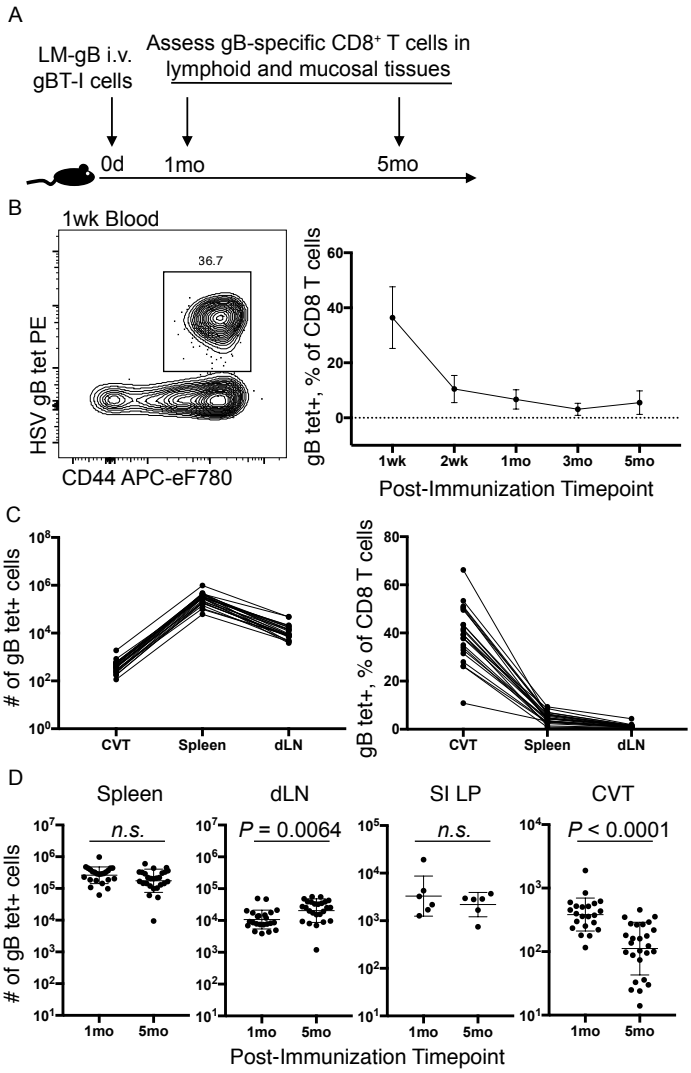
A
LM-gB i.v.
gBT-I cells
Assess gB-specific CD8+ T cells in
lymphoid and mucosal tissues
0d
1mo
5mo
B
1wk Blood
36.7
HSV gB tet PE
CD44 APC-eF780
gB tet+, % of CD8 T cells
1wk
2wk
1mo
3mo
5mo
Post-Immunization Timepoint
C
# of gB tet+ cells
CVT
Spleen
dLN
gB tet+, % of CD8 T cells
D
Spleen
dLN
SI LP
CVT
n.s.
P = 0.0064
n.s.
P < 0.0001
# of gB tet+ cells
1mo
5mo
Post-Immunization Timepoint

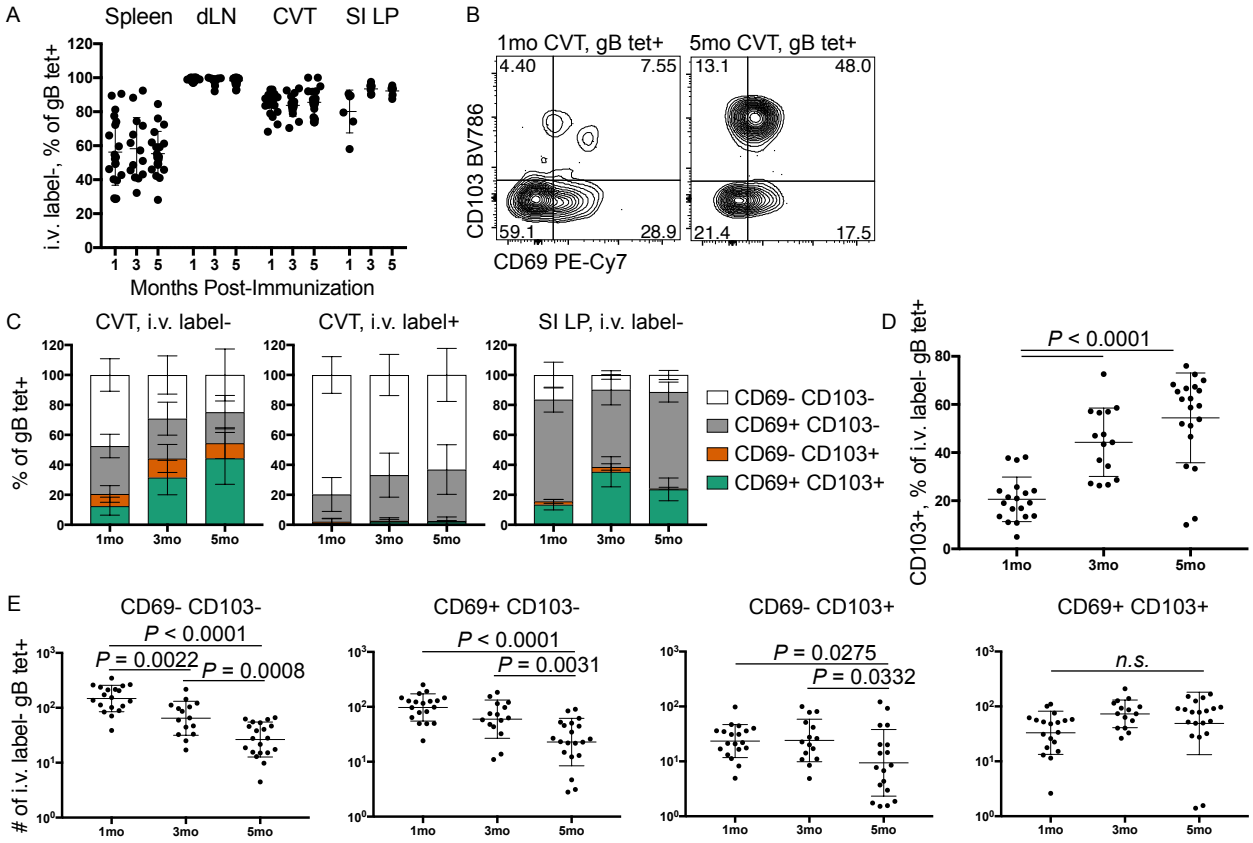
A
Spleen
dLN
CVT
SI LP
i.v. label-, % of gB tet+
Months Post-Immunization
B
1mo CVT, gB tet+
5mo CVT, gB tet+
4.40
7.55
59.1
28.9
13.1
48.0
21.4
17.5
CD103 BV786
CD69 PE-Cy7
C
CVT, i.v. label-
CVT, i.v. label+
SI LP, i.v. label-
% of gB tet+
1mo
3mo
5mo
CD69- CD103-
CD69+ CD103-
CD69- CD103+
CD69+ CD103+
D
P < 0.0001
CD103+, % of i.v. label- gB tet+
E
CD69- CD103-
CD69+ CD103-
CD69- CD103+
CD69+ CD103+
P < 0.0001
P = 0.0022
P = 0.0008
P < 0.0001
P = 0.0031
P = 0.0275
P = 0.0332
n.s.
# of i.v. label- gB tet+

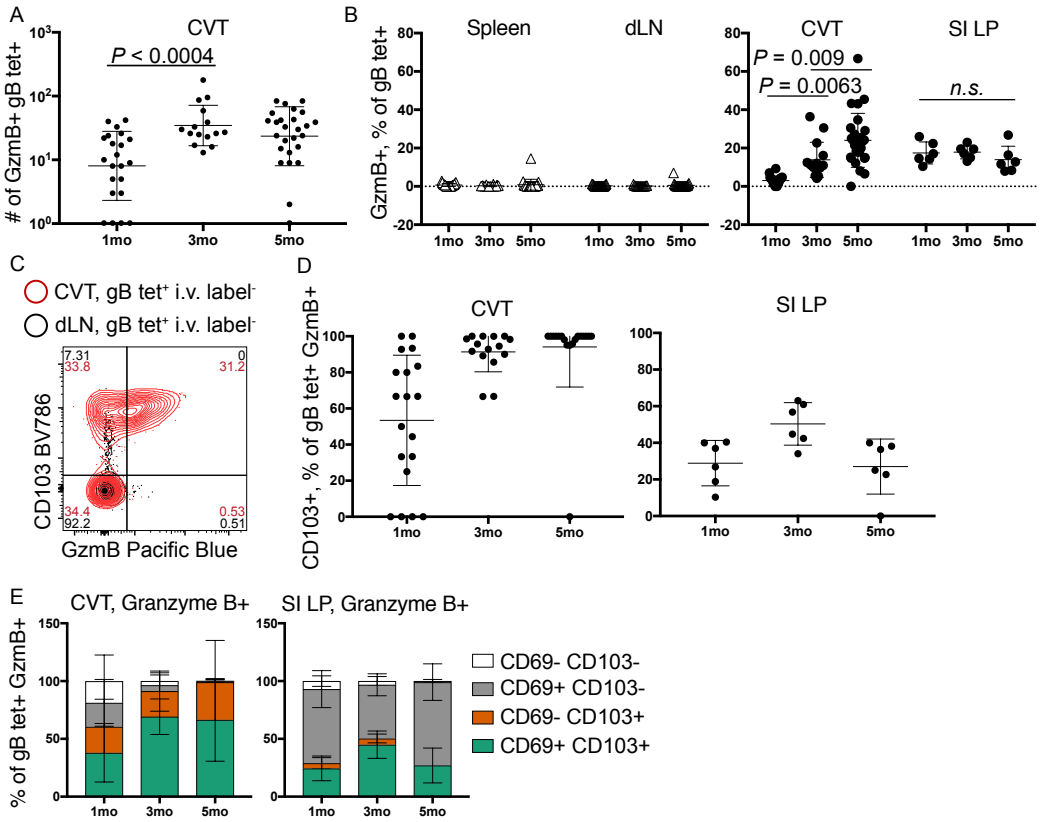
A
CVT
P < 0.0004
# of GzmB+ gB tet+
1mo
3mo
5mo
B
Spleen
dLN
CVT
SI LP
P = 0.009
P = 0.0063
n.s.
GzmB+, % of gB tet+
C
CVT, gB tet+ i.v. label-
dLN, gB tet+ i.v. label-
CD103 BV786
GzmB Pacific Blue
D
CVT
SI LP
CD103+, % of gB tet+ GzmB+
E
CVT, Granzyme B+
SI LP, Granzyme B+
% of gB tet+ GzmB+
CD69- CD103-
CD69+ CD103-
CD69- CD103+
CD69+ CD103+

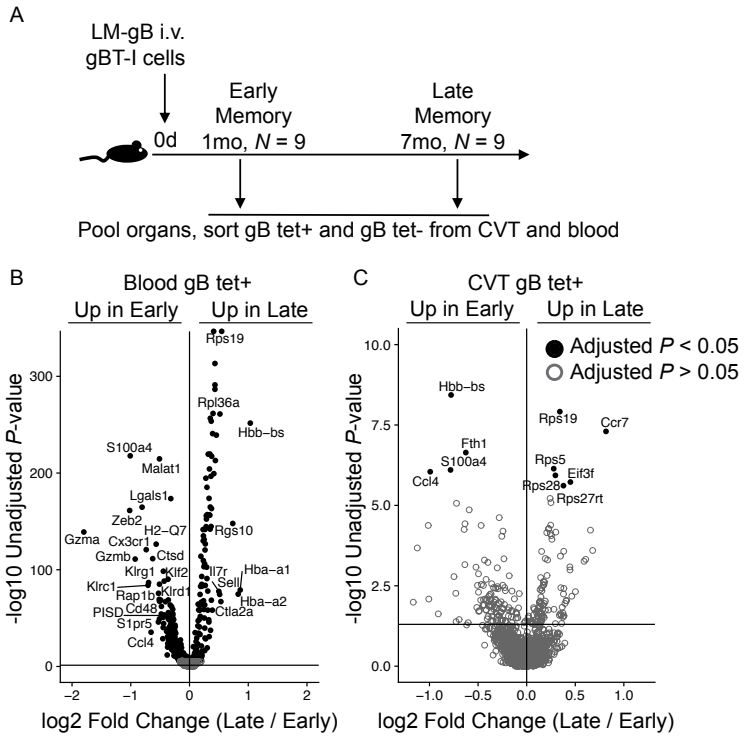
A
LM-gB i.v.
gBT-I cells
0d
Early
Memory
1mo, N = 9
Late
Memory
7mo, N = 9
Pool organs, sort gB tet+ and gB tet- from CVT and blood
B
Blood gB tet+
Up in Early
Up in Late
-log10 Unadjusted P-value
log2 Fold Change (Late / Early)
Rps19
Rpl36a
Hbb−bs
S100a4
Malat1
Lgals1
Zeb2
H2−Q7
Rgs10
Gzma
Cx3cr1
Gzmb
Ctsd
Klrg1
Klf2
Il7r
Hba−a1
Klrc1
Rap1b
Klrd1
Sell
Hba−a2
PISD
Cd48
Ctla2a
S1pr5
Ccl4
C
CVT gB tet+
Up in Early
Up in Late
Adjusted P < 0.05
Adjusted P > 0.05
-log10 Unadjusted P-value
log2 Fold Change (Late / Early)
Hbb−bs
Rps19
Ccr7
Fth1
S100a4
Ccl4
Rps5
Eif3f
Rps28
Rps27rt

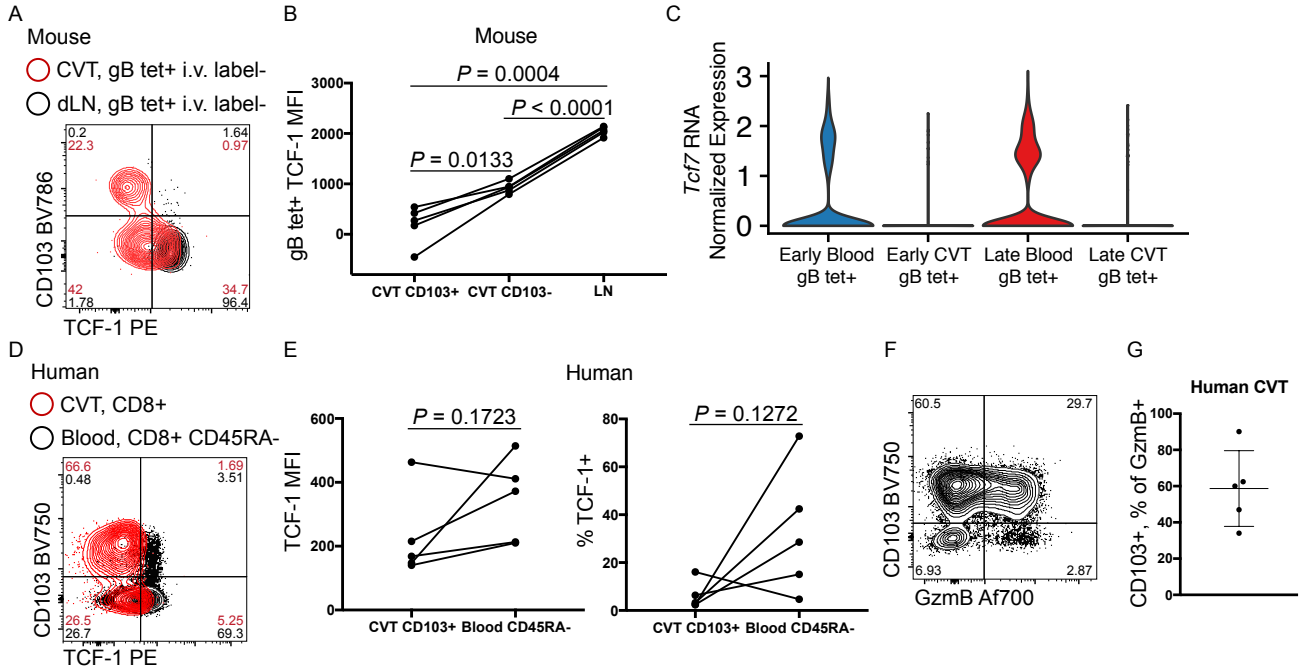
A
Mouse
CVT, gB tet+ i.v. label-
dLN, gB tet+ i.v. label-
CD103 BV786
TCF-1 PE
0.2
22.3
1.64
0.97
42
1.78
34.7
96.4
B
Mouse
P = 0.0004
P < 0.0001
P = 0.0133
gB tet+ TCF-1 MFI
3000
2000
1000
0
CVT CD103+
CVT CD103-
LN
C
Tcf7 RNA
Normalized Expression
3
2
1
0
Early Blood gB tet+
Early CVT gB tet+
Late Blood gB tet+
Late CVT gB tet+
D
Human
CVT, CD8+
Blood, CD8+ CD45RA-
CD103 BV750
TCF-1 PE
66.6
0.48
1.69
3.51
26.5
26.7
5.25
69.3
E
Human
P = 0.1723
TCF-1 MFI
600
400
200
0
CVT CD103+
Blood CD45RA-
P = 0.1272
% TCF-1+
80
60
40
20
0
CVT CD103+
Blood CD45RA-
F
CD103 BV750
GzmB Af700
60.5
29.7
6.93
2.87
G
Human CVT
CD103+, % of GzmB+
100
80
60
40
20
0

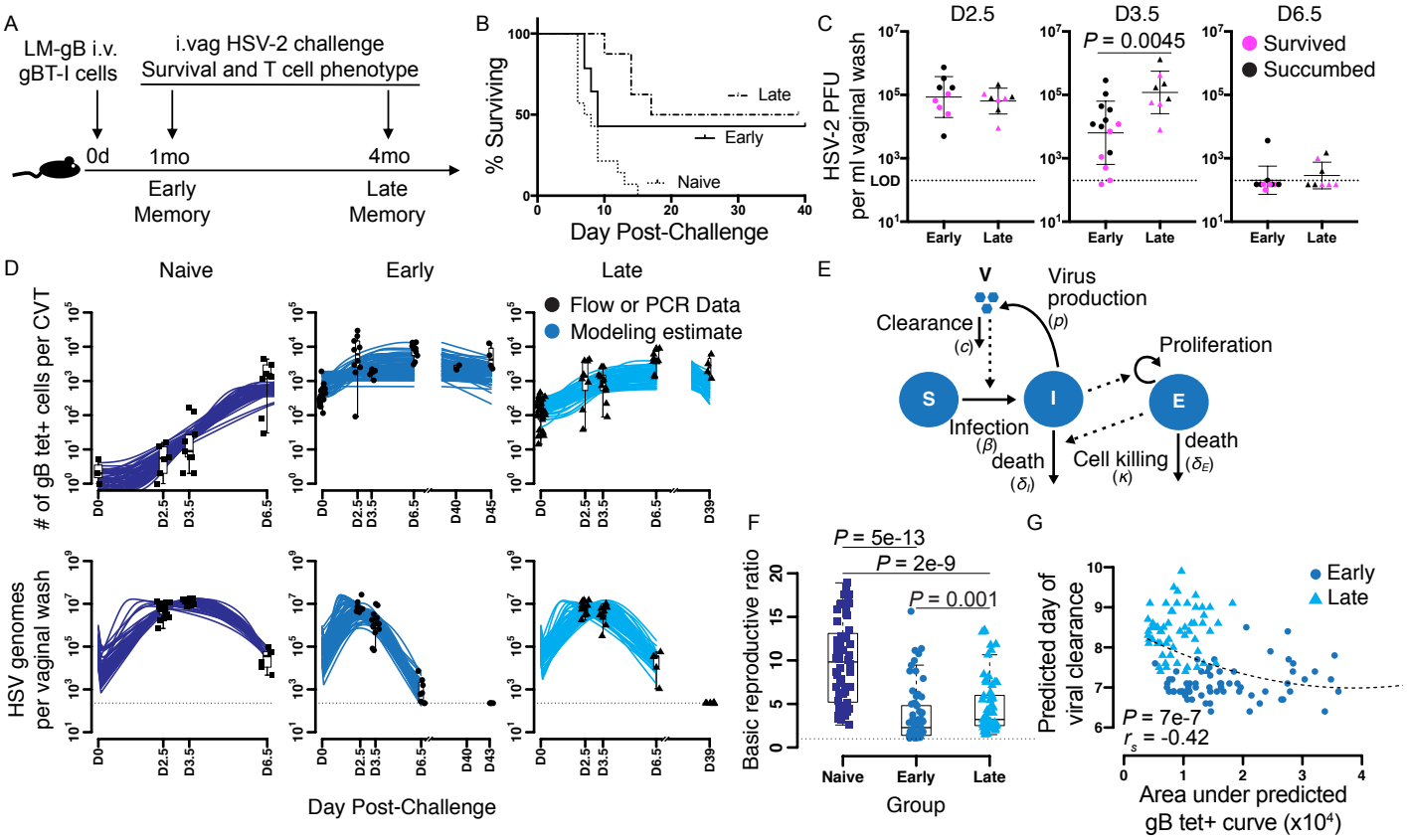
A
LM-gB i.v.
gBT-I cells
i.vag HSV-2 challenge
Survival and T cell phenotype
0d
1mo
4mo
Early Memory
Late Memory
B
% Surviving
Day Post-Challenge
Late
Early
Naive
C
D2.5
D3.5
D6.5
HSV-2 PFU per ml vaginal wash
P = 0.0045
Survived
Succumbed
LOD
Early
Late
D
Naive
Early
Late
Flow or PCR Data
Modeling estimate
# of gB tet+ cells per CVT
HSV genomes per vaginal wash
Day Post-Challenge
E
V
Virus production
(p)
Clearance
(c)
Proliferation
S
I
E
Infection
(β)
death
(δI)
Cell killing
(κ)
death
(δE)
F
P = 5e-13
P = 2e-9
P = 0.001
Basic reproductive ratio
Naive
Early
Late
Group
G
Early
Late
Predicted day of viral clearance
P = 7e-7
rs = -0.42
Area under predicted gB tet+ curve (x10⁴)